Inclusive Quarkonium Production at ATLAS and CMS

Tamar Zakareishvili[1*],
[1] IFIC, CSIC-UV - currently
* HEPI TSU - PhD work

Quarkonia as Tools 2024
8.01.2024

Supported by AEI grant: PID2021-124912NB-I00

Outline

- This talk will mostly cover recent ATLAS measurements - covering the transverse momentum range well beyond previously achieved!
- Compare to the latest CMS and ALICE measurements.

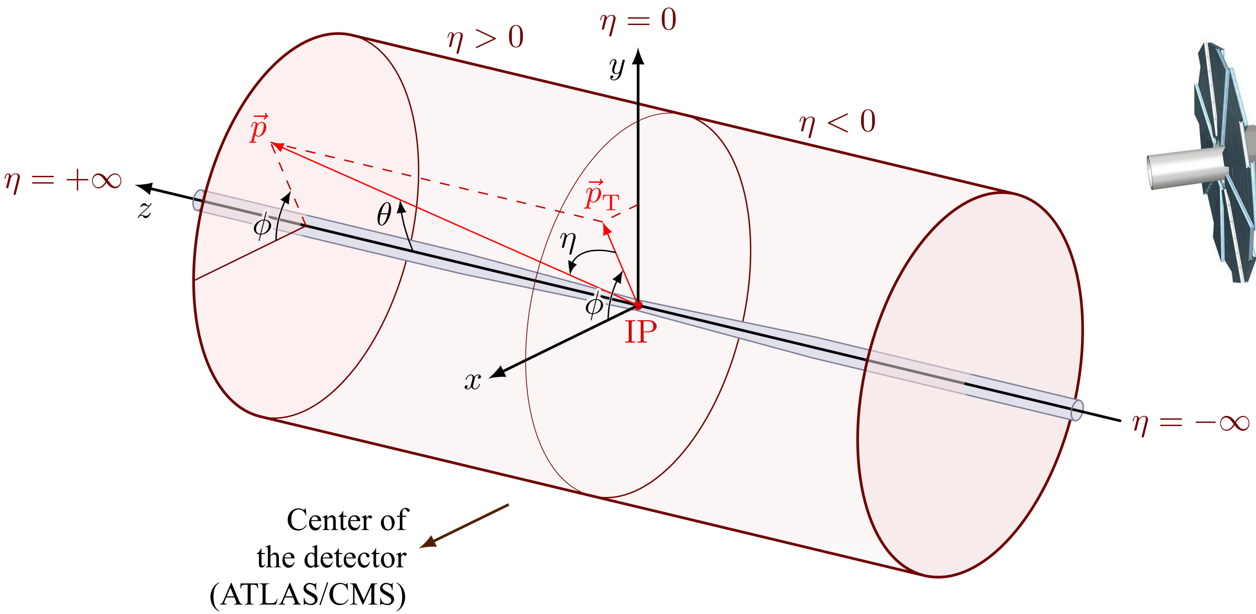

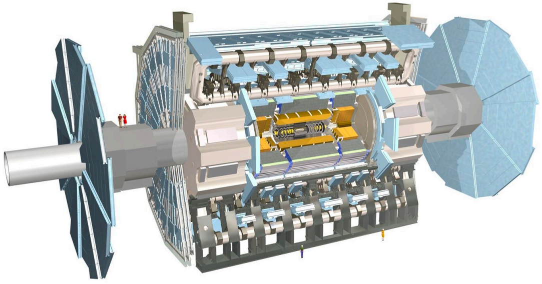

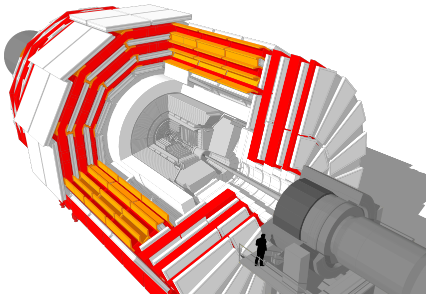

Quarkonium - motivation to study it

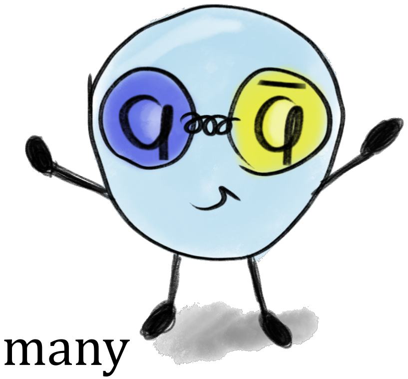

- Quarkonium - bound state of a quark and anti-quark
- Despite long history, hadronic production of quarkonium still poses many questions.
- Need to expand further the variety of experimental inputs to help theoretical understanding.
- While the theoretical calculations within the framework of perturbative QCD have been reasonably successful in describing the non-prompt contributions, a satisfactory understanding of the prompt production mechanisms is still to be achieved.
- It is hence increasingly important to broaden the scope of comparison between theory and experiment by providing a broader variety of experimental information on quarkonium production in a wider kinematic range.

Production mechanism

At the LHC - two major mechanisms: prompt (from short-lived QCD sources) and non-prompt (from B hadron decays).

Prompt Quarkonium: produced directly in the primary interaction point (pp collision - created promptly during the collision process and are associated with the hard scatter of partons involved in the collision).

Non-prompt Quarkonium: produced indirectly, typically through the decay of B mesons -> they have a finite lifetime, the quarkonium states originating from their decay are referred to as non-prompt because there is a delay (in time and space) between the initial collision and the formation of the quarkonium state.

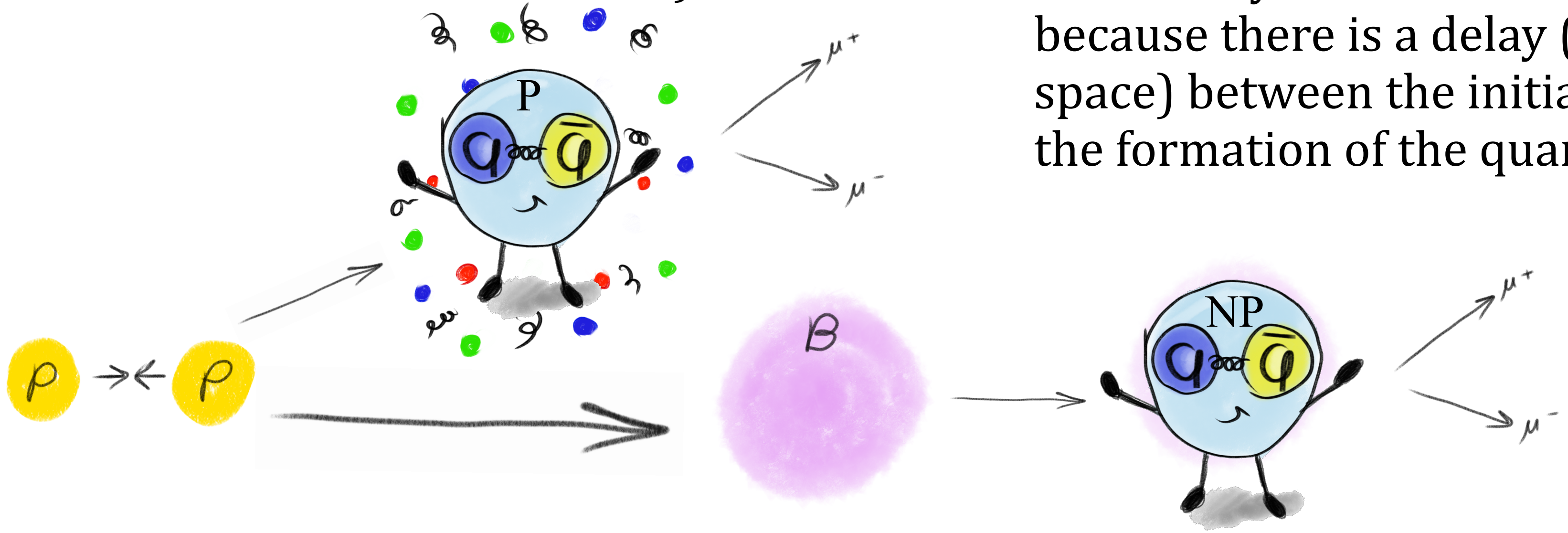

Measurement strategy

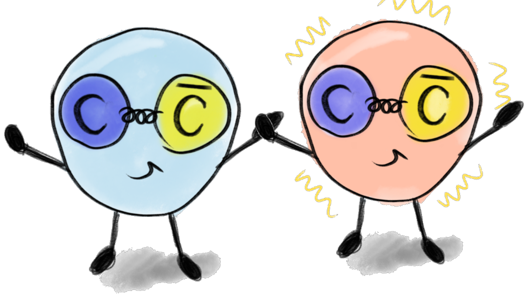

Important notions in the analysis:

- **Acceptance** - the fraction of events or particles that are successfully detected or measured within the designed geometrical and kinematic constraints of a detector.
- **Triggering** - selecting and recording events that fulfil specific criteria in real-time during data acquisition.
- **Efficiency** corrections:

  - Corrections are applied to account for acceptance and trigger inefficiencies.

  - Correction factors are determined through the studies using control samples and simulation.

Goal is to measure the **production cross-section** of charmoniums ($c\bar{c}$): J/ψ and ψ(2S) mesons in pp collisions.

- Channel: $\psi \rightarrow \mu^+\mu^-$
- Separate prompt and non-prompt contributions;
- Cover wide range of transverse momentum for J/ψ and ψ(2S) by combining two triggers:
  - Low p_T range: $8 < p_T < 60$ GeV - di-muon trigger 2mu4 - 2015 data;
  - High p_T range: $60 < p_T < 360$ GeV - single muon trigger mu50 - Run 2 data.

Measurement strategy

- The prompt (P) and non-prompt (NP) double-differential production cross sections for $\psi = J/\psi, \psi(2S)$ are calculated as follows:

$$\frac{d^2\sigma^{P,NP}(pp \to \psi)}{dp_{\mathrm{T}}dy} \times \mathcal{B}(\psi \to \mu^+\mu^-) = \frac{1}{\mathcal{A}(\psi)\epsilon_{\mathrm{trig}}\epsilon_{\mathrm{trigSF}}\epsilon_{\mathrm{reco}}\epsilon_{\mathrm{recoSF}}} \frac{N_{\psi}^{P,NP}}{\Delta p_{\mathrm{T}}\, \Delta y\, \int \mathcal{L}dt}$$

- A(ψ) - the geometrical acceptance calculated separately for low p T and high p T bins, using the cuts:
  - in low p_{T} range: p_{T} ($\mu 1$) > 4 GeV, p_{T} ($\mu 2$) > 4 GeV, $|\eta(\mu 1), \eta(\mu 2)| < 2.4$
  - in high p_{T} range: p_{T} ($\mu 1$) > 52.5 GeV, p_{T} ($\mu 2$) > 4 GeV, $|\eta(\mu 1), \eta(\mu 2)| < 2.4$
- ϵ_{trig} - the trigger efficiency, calculated using MC Monte Carlo samples.
- $\epsilon_{\mathrm{trigSF}}$ - the trigger correction scale factor accounting for MC-data differences.
- ϵ_{reco} - the reconstruction efficiency, calculated using the Monte Carlo samples.
- $\epsilon_{\mathrm{recoSF}}$ - the reconstruction efficiency correction scale factor accounting for MC-data differences.
- $N_{\psi}^{\mathrm{P,NP}}$ - the raw yields of J/ψ and $\psi(2S)$, obtained from 2D maximum likelihood fits.
- Δp_{T} and Δy - corresponding bin widths in p_{T} and absolute rapidity.
- $\int \mathrm{L}dt$ - the corresponding integrated luminosity.

Important variables

ψ candidates - di-muon system.
Important variables: ψ candidate mass and pseudo-proper time

J/ψ candidates are distinguished from ψ(2S) through the mass peak.

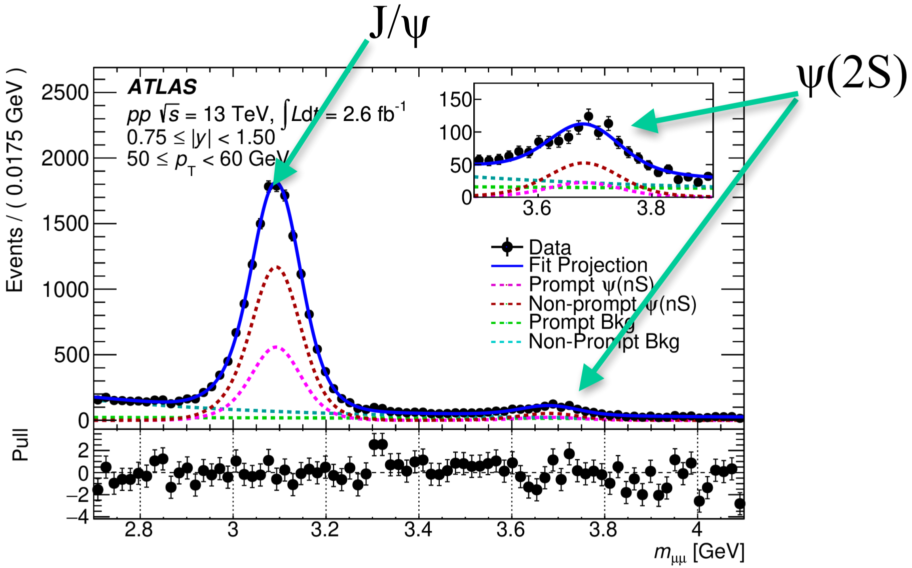

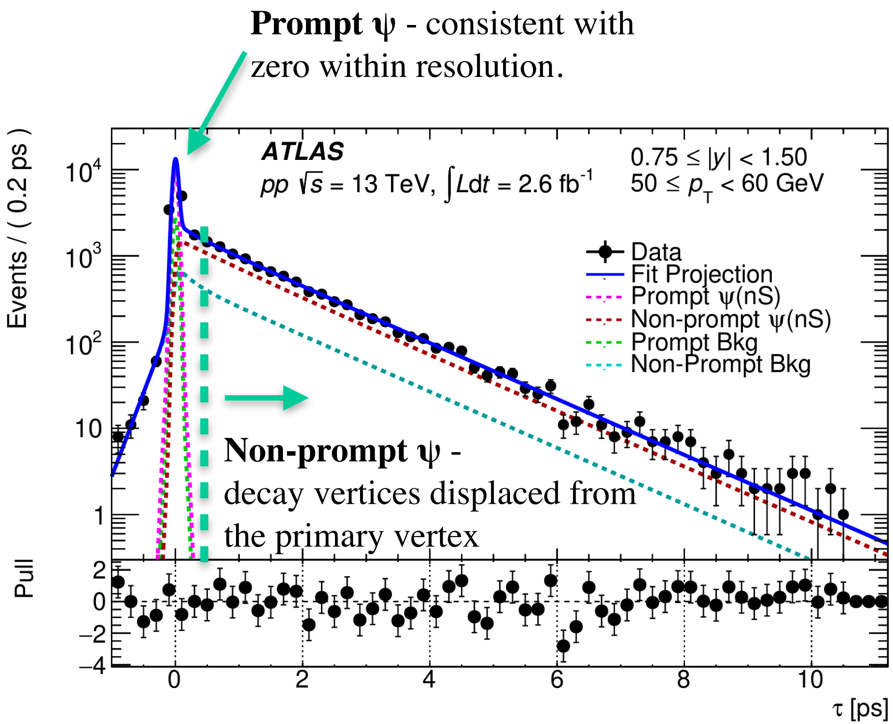

Prompt ψ candidates are distinguished from those originating from b-hadron decays through the separation of the primary vertex and the J/ψ decay vertex. The pseudo-proper time:

$$\tau = \frac{m_{\mu\mu}}{p_{\mathrm{T}}} \frac{L_{xy}}{c}$$

p_{T} - dimuon transverse momentum

L_{xy} - transverse distance between primary and dimuon vertex

c - speed of light

Fit model

2D unbinned maximum likelihood fit is done to obtain raw yields - $N_{\psi}^{P,NP}$. The fit model is described by a sum of the following terms:

$$PDF(m,\tau) = \sum_{i=1}^{7} \kappa_i f_i(m) \cdot (h_i(\tau) \otimes R(\tau)) \cdot C_i(m,\tau).$$

m - dimuon invariant mass
τ - pseudo-proper lifetime of the dimuon
R(τ) - experimental resolution in pseudo-proper lifetime - sum of three Gaussians

i	Type	P/NP	$f_i(m)$	$h_i(\tau)$	$C_i(m,\tau)$
1	J/ψ	P	$\omega_0 G_1^{'}(m) + (1-\omega_0)[\omega_1 CB_1^{'}(m) + (1-\omega_1)G_1^{''}(m)]$	$\delta(\tau)$	$BV(m,\tau,\rho)$
2	J/ψ	NP	$\omega_0 G_1^{'}(m) + (1-\omega_0)[\omega_1 CB_1^{'}(m) + (1-\omega_1)G_1^{''}(m)]$	$\omega_2 E_1(\tau) + (1-\omega_2)E_1^{'}(\tau)$	1
3	$\psi(2S)$	P	$\omega_0 G_2^{'}(m) + (1-\omega_0)[\omega_1 CB_2^{'}(m) + (1-\omega_1)G_2^{''}(m)]$	$\delta(\tau)$	1
4	$\psi(2S)$	NP	$\omega_0 G_2^{'}(m) + (1-\omega_0)[\omega_1 CB_2^{'}(m) + (1-\omega_1)G_2^{''}(m)]$	$E_2(\tau)$	1
5	Bkg	P	B	$\delta(\tau)$	1
6	Bkg	NP	$E_4(m)$	$E_5(\tau)$	1
7	Bkg	NP	$E_6(m)$	$E_7(\lvert\tau\rvert)$	1

Notation	Function
G	Gaussian
CB	Crystal Ball
E	Exponential
B	Bernstein polynomials
BV	Correlation term of the bivariate Gaussian dist.

- The same fit model is used throughout the full kinematic range.
- Pull distributions and 2D Chi^2 values are calculated to assess fit quality.

Some fit examples

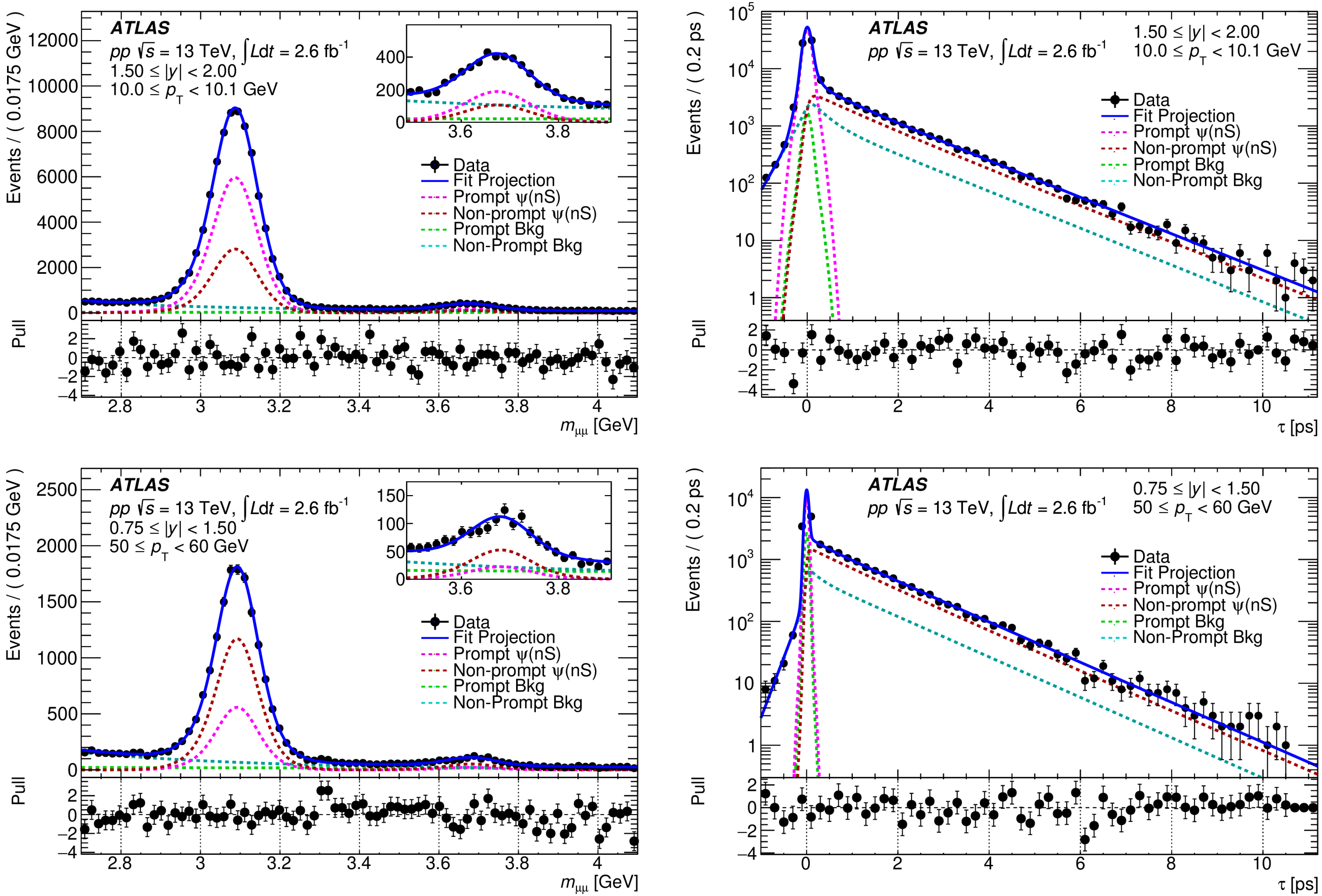

Some fit examples

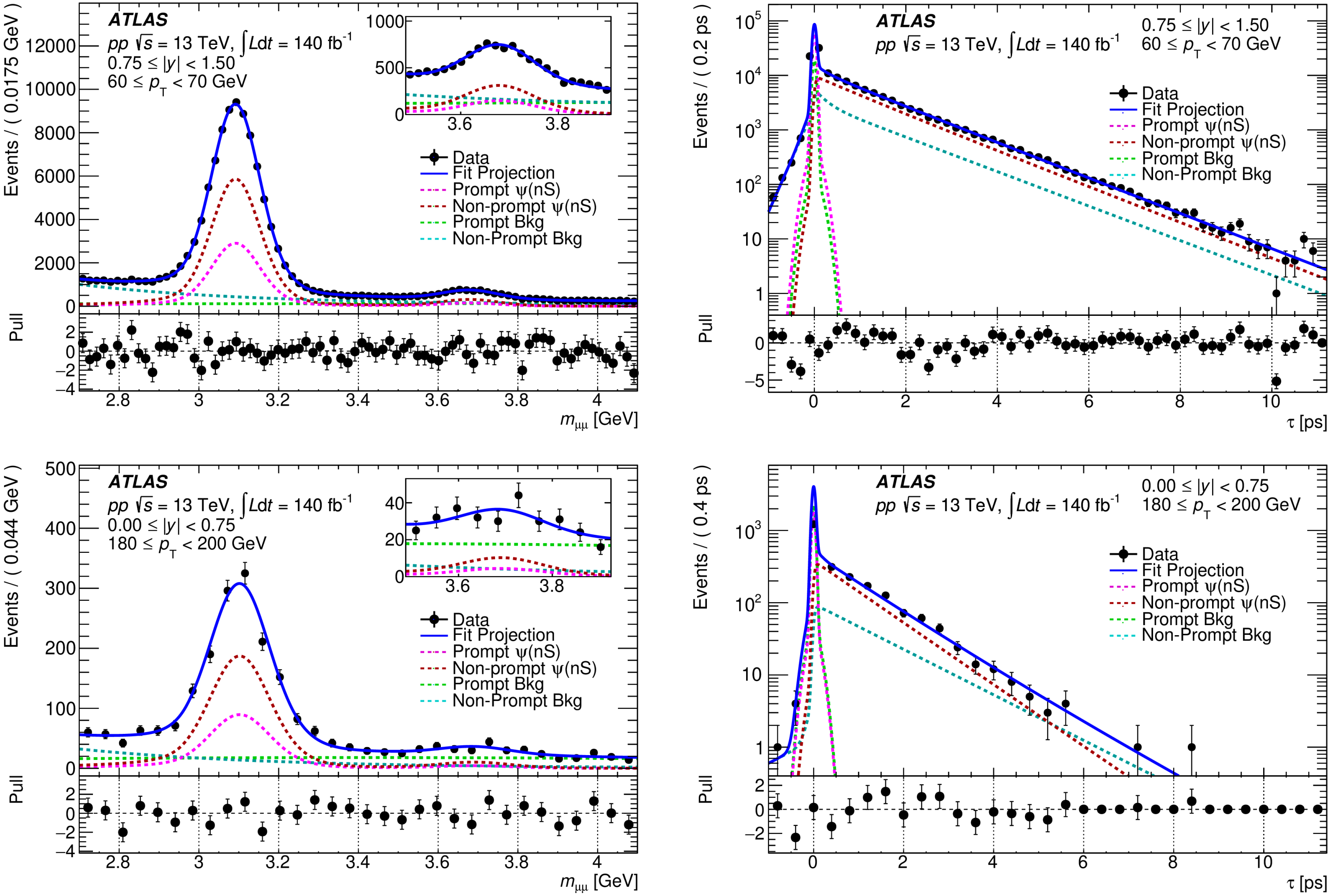

Systematic studies

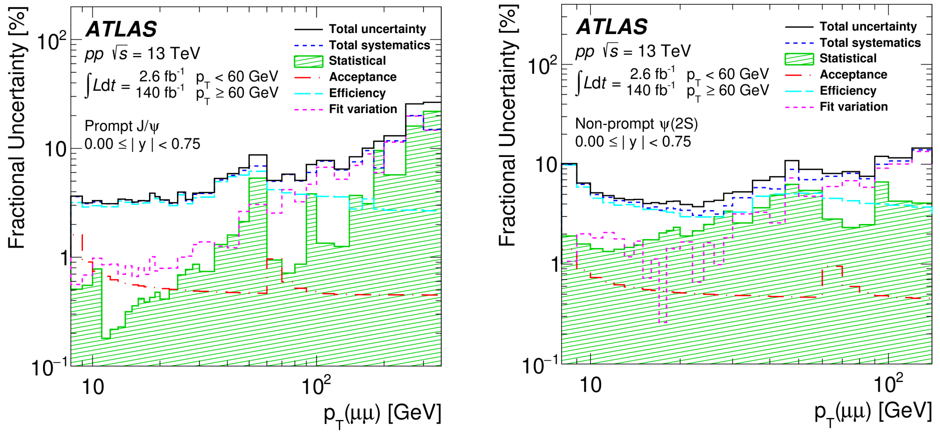

The fractional uncertainty contributions of the differential prompt J/ψ (left) and $\psi(2S)$ (right) cross-section.

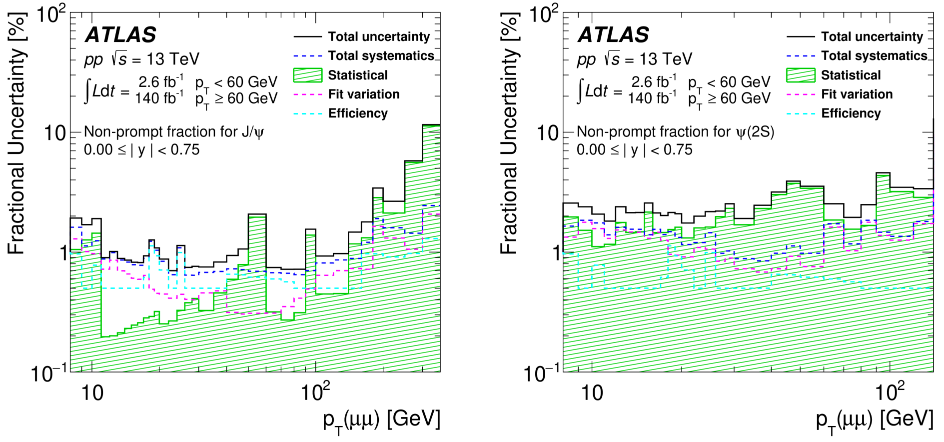

The fractional uncertainty contributions of the non-prompt fraction of J/ψ (left) and $\psi(2S)$ (right).

Sources of systematics:

1. Acceptance systematics.
2. Efficiency systematics (Trigger + Reconstruction).
3. Fit model systematics.
4. Luminosity uncertainty.
5. Spin alignment correction factors.

Trends visible on the plots due to:

- statistical effects
- change of the trigger

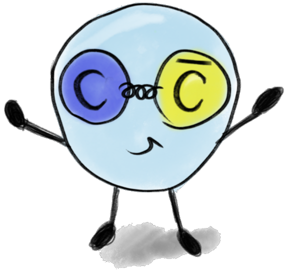

J/ψ cross-section

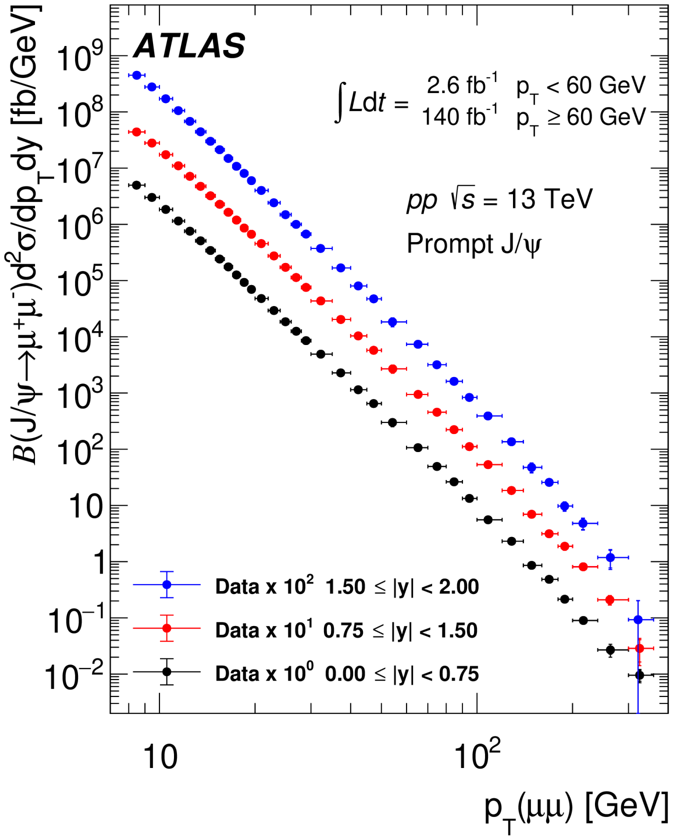

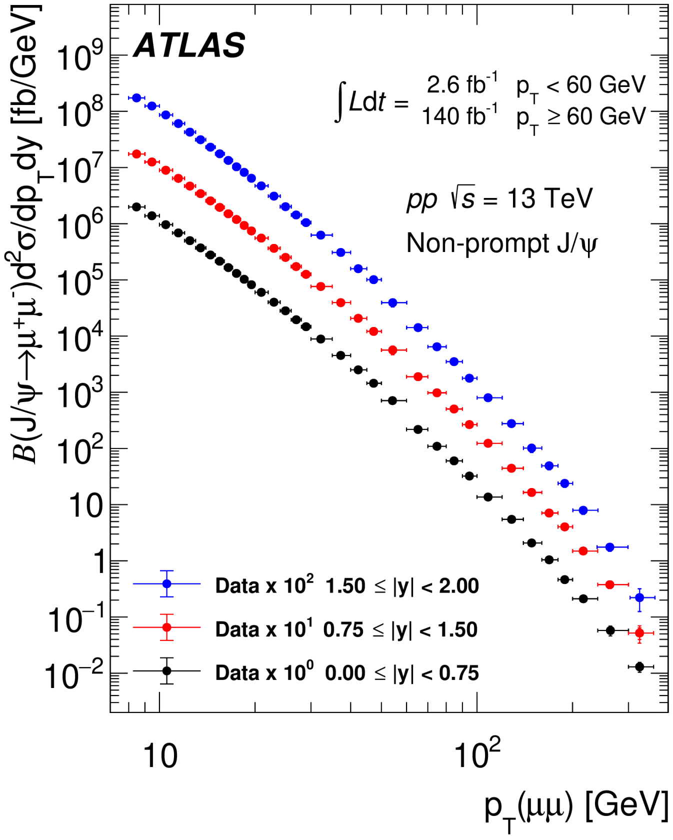

- The measured double-differential cross-sections for prompt and non-prompt J/ψ production in the nominal isotropic spin-alignment scenario.
- For visual clarity, a scaling factors are applied to the rapidity slices.

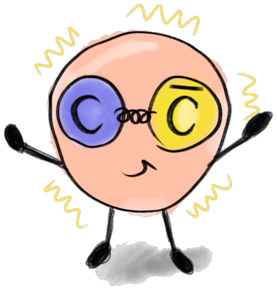

ψ(2S) cross-section

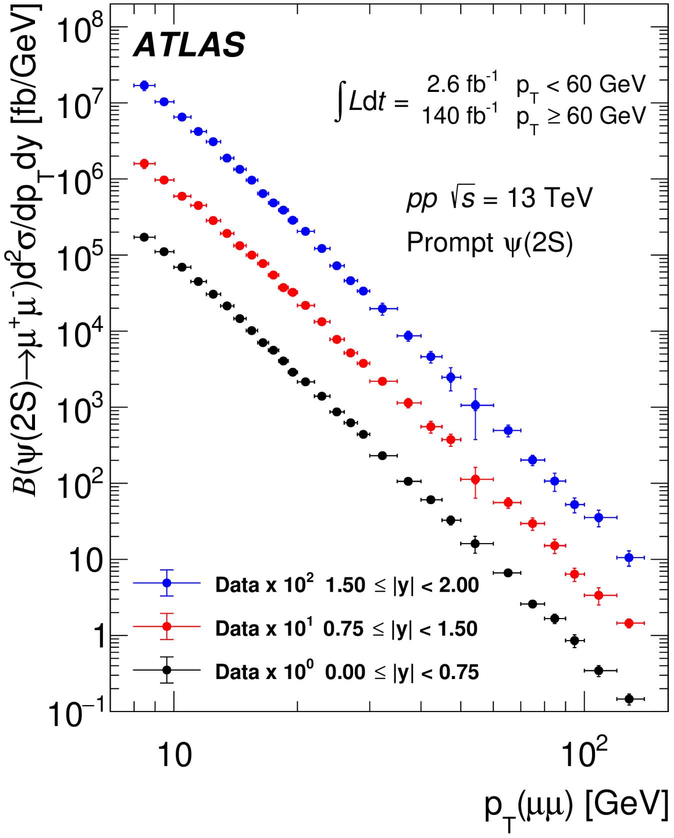

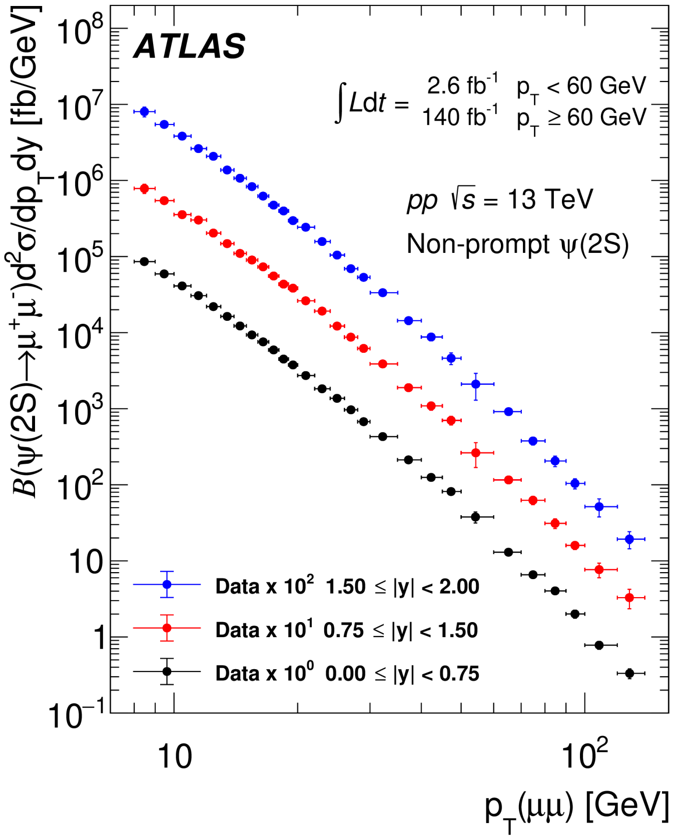

- The measured double-differential cross-sections for prompt and non-prompt $\psi(2S)$ production in the nominal isotropic spin-alignment scenario.
- For visual clarity, a scaling factors are applied to the rapidity slices.

Production ratio plots

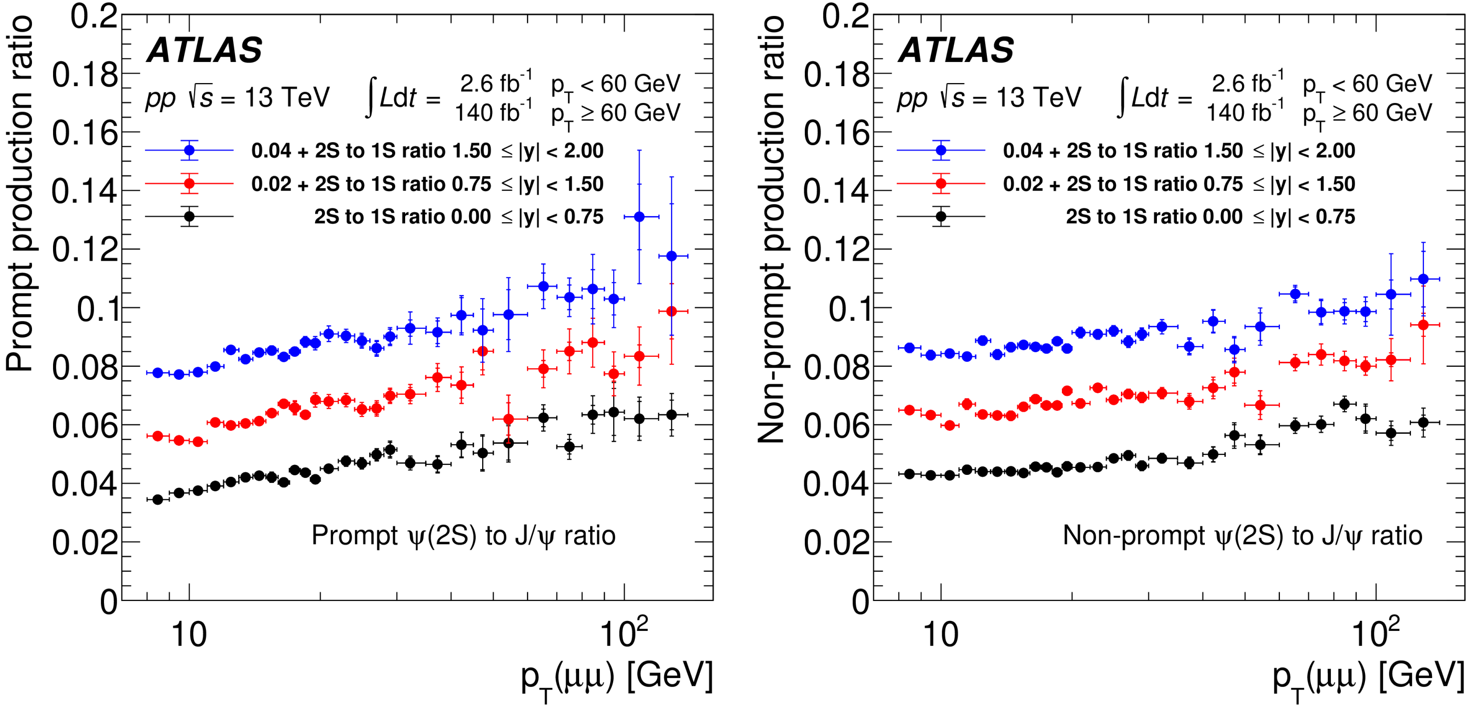

- The $\psi(2S)$-to-J/ψ production ratio for the prompt and non-prompt production mechanisms
- For visual clarity, vertical shifts are applied to the rapidity slices.
- Slightly different slopes for Prompt and Non-prompt production.

Non-prompt fraction plots

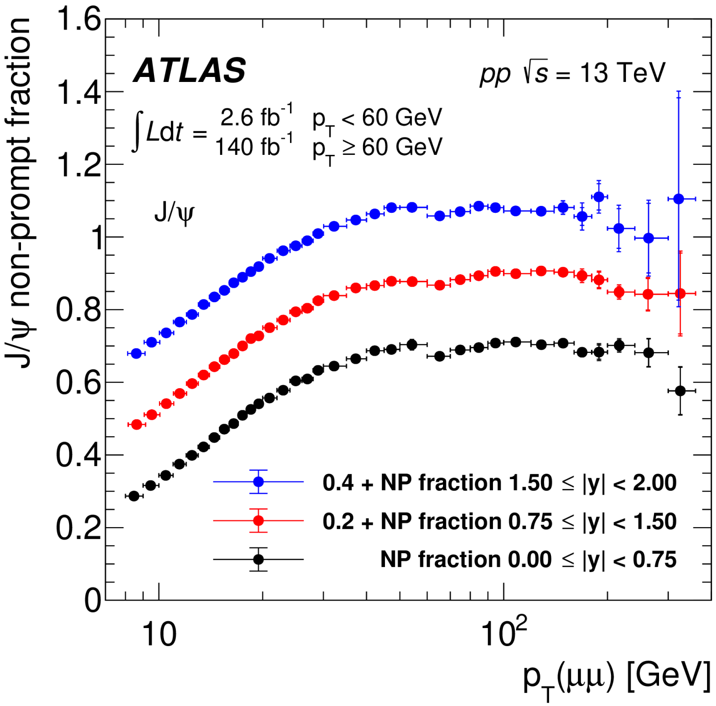

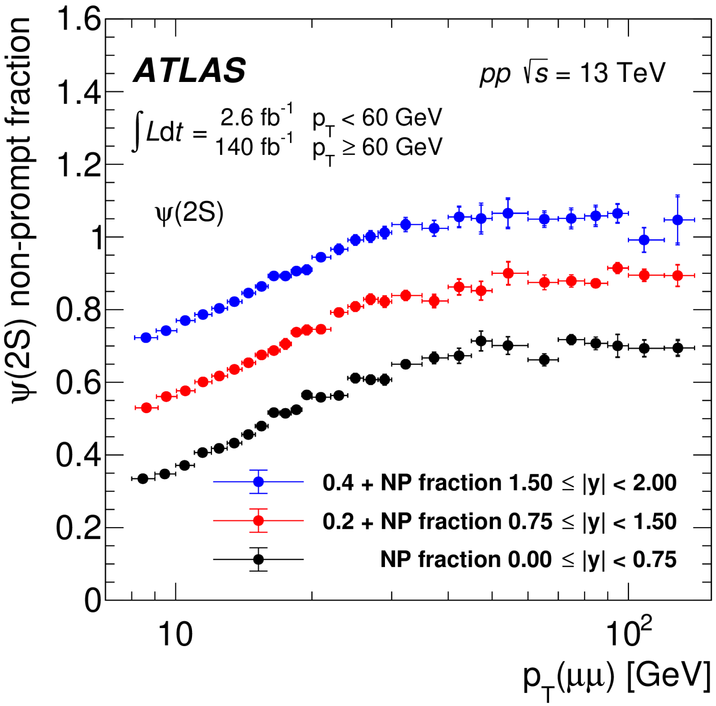

- Non-prompt production fraction of J/ψ and $\psi(2S)$ mesons
- For visual clarity, vertical shifts are applied to the rapidity slices.
- The non-prompt fractions increase steadily with pT up to about 100 GeV
- almost constant for both J/ψ and $\psi(2S)$ in the high pT range,
- similar pT-dependences for the prompt and non-prompt differential cross-sections at very high transverse momenta.

- The transition boundary at pT = 60 GeV between the low- pT dimuon trigger and the high- pT single-muon trigger areas represents a particular challenge because of the sharp change in event kinematics.

Spin alignment hypothesis corrections

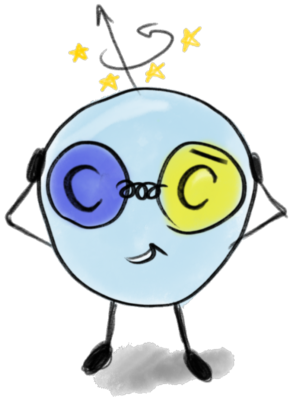

Most general angular dependence for ψ → mu⁺mu⁻ decay:

$$\frac{d^2N}{d\cos\theta^\star d\phi^\star} \propto 1 + \lambda_\theta \cos^2\theta^\star + \lambda_\phi \sin^2\theta^\star \cos 2\phi^\star + \lambda_{\theta\phi} \sin 2\theta^\star \cos\phi^\star$$

- The coefficients λ_θ , λ_ϕ and $\lambda_{\theta\phi}$ are related to the spin-density matrix elements of the dimuon spin wave function for various polarisations.
- It was found that the dependence of acceptance on parameters λ_ϕ and $\lambda_{\theta\phi}$ is very weak, while dependence on λ_θ can be significant.
- For illustrating more realistic correction factors, it was decided to produce graphs with correction factors corresponding to the variation of λ_θ between +/-0.2, reflecting the level of experimental knowledge on this coefficient.

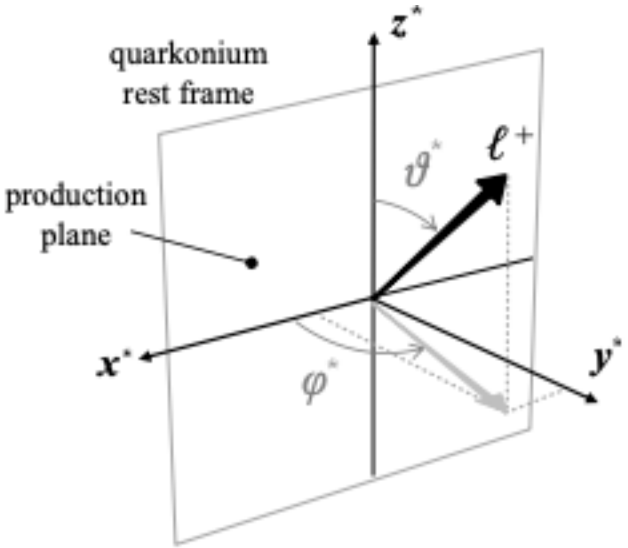

Figure from P. Faccioli

Spin alignment hypothesis corrections

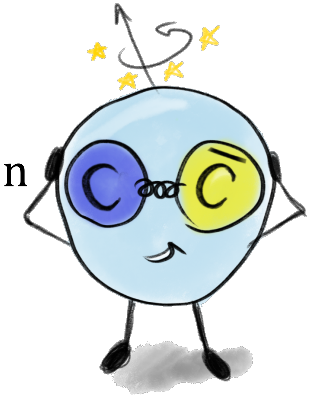

- Spin alignment of ψ states may be different for prompt and non-prompt production mechanisms - additional correction factors may be needed for all measured distributions.
- Correction factors were calculated for a variety of scenarios. It was found that the dependence on polar angle θ in the helicity frame of ψ state results in the largest variation, so the angular dependence of f $\psi \rightarrow \mu + \mu -$ decays is assumed to be $\propto (1 + \lambda_\theta \cos^2\theta)$.

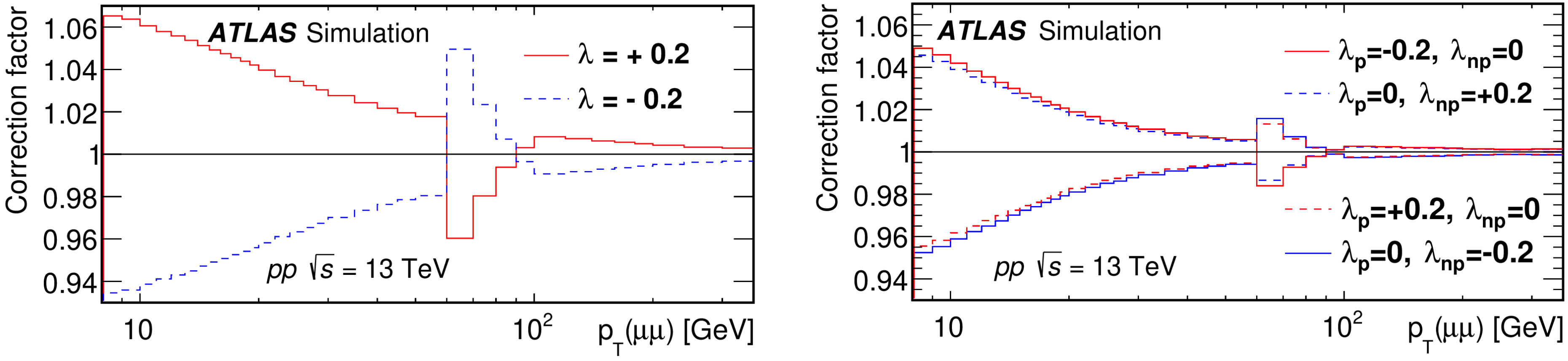

Spin alignment hypothesis correction factors for the differential cross sections (left plot) and non-prompt fractions (right plot), where the values $\lambda = \pm 0.20$.

Theory comparison: prompt J/ψ and ψ(2S) production

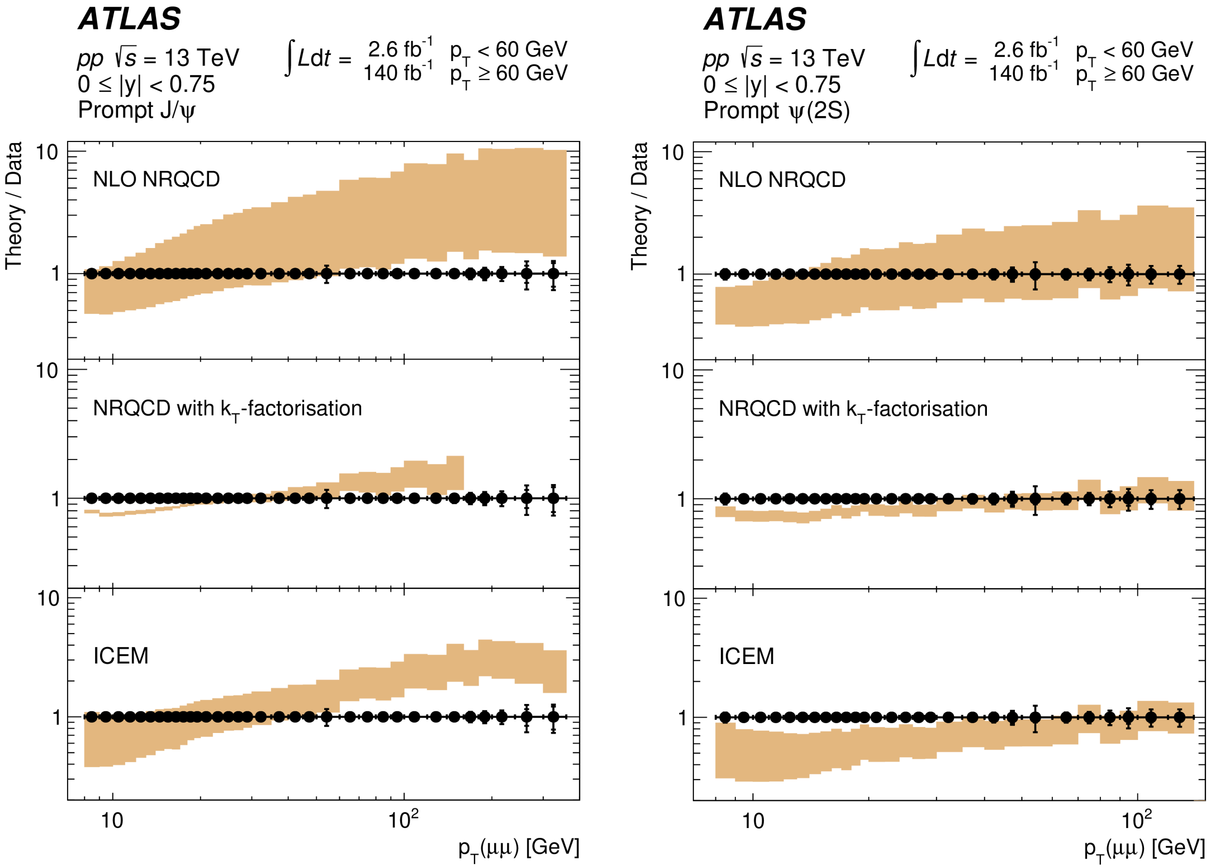

- Model calculations of prompt production of charmonium are usually based on perturbative QCD for the production of the $c\bar{c}$ pair, and differ in the mechanism of formation of the bound state with specific quantum numbers.
- Model **NLO NRQCD** [1-3]- largely overlap with the data points within theoretical uncertainties, with increasing p_T prediction seem to fall more slowly than the data.
- k_T **-factorisation** [4-7] - where available this model reproduce the shapes of the measured p_T distributions reasonably well, but tend to underestimate the cross sections at low p_T.
- **Improved Colour Evaporation Model (ICEM)** [8] - model seems to expect harder p_T spectra than observed in the data for both J/ψ and $\psi(2S)$, and tends to underestimate the cross section for $\psi(2S)$.

Theory comparison: non-prompt J/ψ and ψ(2S) production

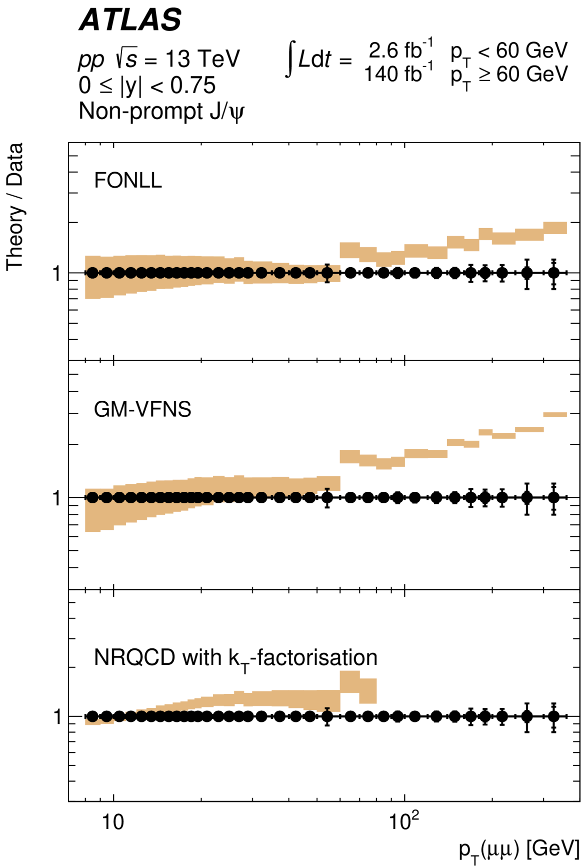

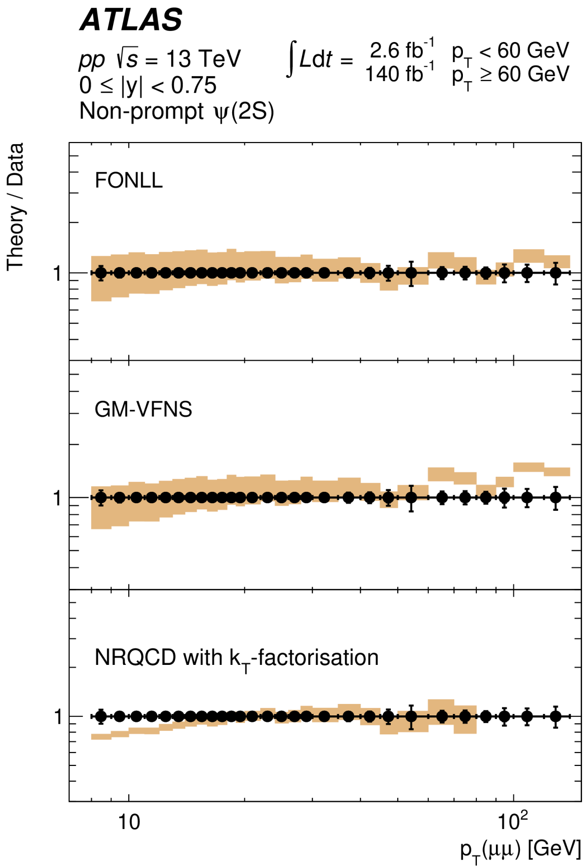

- Theoretical calculations of non-prompt charmonium production - based on perturbative QCD for the production of a $b\bar{b}$ quark pair, their hadronisation into a pair of B hadrons, and their subsequent decay into a charmonium state with specific quantum numbers.
- Fixed-order-next-to-leading-log (**FONLL**) [9-11] QCD calculations are in a good agreement at lower p_{T}, but the model predicts somewhat higher cross-sections for J/ψ at the high p_{T} end.
- **GM-VFNS** (general-mass variable-flavor- number scheme) model [12-14]- achieves similar results, but the deviation from data at the highest p_{T} is somewhat more pronounced.
- k_T **-factorisation** [6,15] model - the cross section for $\psi(2S)$ non-prompt production at low p_{T} is somewhat underestimated.

Neither model is able to accurately describe the data across the entire transverse momentum range.

Prompt J/ψ cross-section comparison - central rapidity

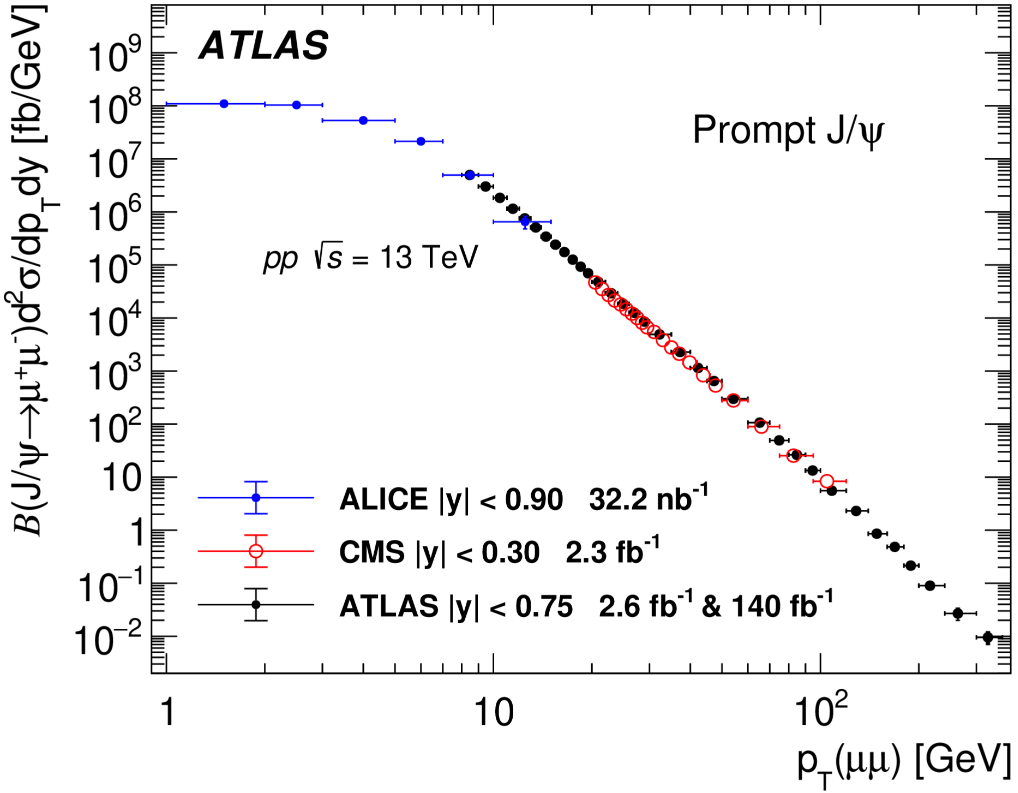

- ALICE results in [1 – 15] GeV (32.2 nb^{-1}) JHEP 03 (2022) 190
- CMS results in [20 – 120] GeV (2.3 fb^{-1}) Phys. Lett. B 780 (2018) 251
- ATLAS measurement results in [8 – 360] GeV (2.6 fb^{-1} / 139 fb^{-1}) CERN-EP-2023-193
- Different experiment results seem to coincide nicely in matching ranges!

Summary

- Discussed the procedure and the results of a measurement of J/ψ and $\psi(2S)$ production, using the ATLAS detector and the full Run 2 data set collected with pp collisions at 13 TeV.
  - Measured, separately for prompt and non-prompt production mechanisms:
    - Double differential cross-sections for J/ψ and $\psi(2S)$;
    - Non-prompt fractions of J/ψ and $\psi(2S)$;
    - production ratios of $\psi(2S)$ to J/ψ.
  - Covered the range of rapidities between -2 and $+2$:
    - for J/ψ covered p_T range: 8 to 360 GeV;
    - for $\psi(2S)$ covered p_T range: 8 to 140 GeV.
  - **Covered transverse momentum range is well beyond what was previously achieved!**
- **ATLAS results are consistent** with similar results obtained by the **CMS** collaboration**,** and **ALICE** collaboration.
- Number of theoretical predictions for both Prompt and Non-prompt were compared to the ATLAS results - they describe the data with varying levels of success.

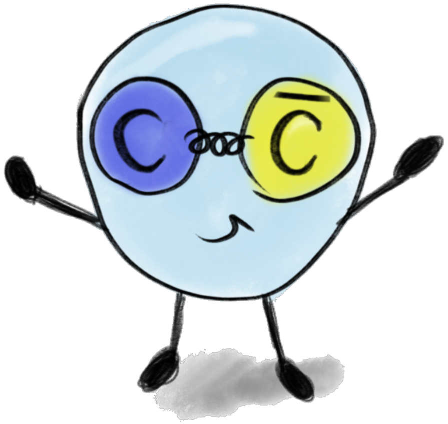

Thank you!

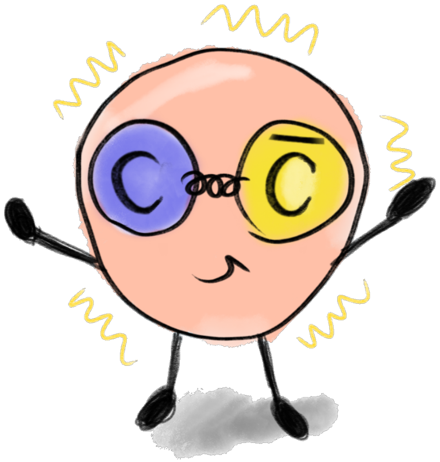

Backup

References

[1] M. Butenschön and B. A. Kniehl, Reconciling J/ψ Production at HERA, RHIC, Tevatron, and LHC with Nonrelativistic QCD Factorization at Next-to-Leading Order, Phys. Rev. Lett. 106 (2011) 022003.

[2] M. Butenschoen and B. A. Kniehl, World data of J/ψ production consolidate nonrelativistic QCD factorization at next-to-leading order, Phys. Rev. D 84 (2011) 051501.

[3] M. Butenschoen and B. A. Kniehl, Global analysis of ψ(2S) inclusive hadroproduction at next-to-leading order in nonrelativistic-QCD factorization, Phys. Rev. D 107 (2023) 034003, arXiv: 2207.09346.

[4] S. P. Baranov, A. V. Lipatov and N. P. Zotov, Prompt charmonia production and polarization at LHC in the NRQCD with kT -factorization. Part I: $\psi(2S)$ meson, Eur. Phys. J. C 75 (2015) 455, arXiv: 1508.05480 [hep-ph].

[5] S. P. Baranov and A. V. Lipatov, Prompt charmonia production and polarization at the LHC in the NRQCD with kT-factorization. III. J/ψ meson, Phys. Rev. D 96 (2017) 034019.

[6] A. V. Lipatov, M. A. Malyshev and S. P. Baranov, Particle Event Generator: A Simple-in-Use System PEGASUS version 1.0, Eur. Phys. J. C 80 (2020) 330, arXiv: 1912.04204 [hep-ph].

[7] S. P. Baranov and A. V. Lipatov, Are there any challenges in the charmonia production and polarization at the LHC?, Phys. Rev. D 100 (2019) 114021.

[8] V. Cheung and R. Vogt, Production and polarization of direct J/ψ to O (α 3 s) in the improved color evaporation model in collinear factorization, Phys. Rev. D 104 (2021) 094026.

[9] M. Cacciari, S. Frixione and P. Nason, The pT spectrum in heavy flavor photoproduction, JHEP 03 (2001) 006, arXiv: hep-ph/0102134. 21

[10] M. Cacciari et al., Theoretical predictions for charm and bottom production at the LHC, JHEP 10 (2012) 137, arXiv: 1205.6344 [hep-ph].

[11] M. Cacciari, FONLL Heavy Quark Production, http://www.lpthe.jussieu.fr/~cacciari/fonll/fonllform.html, Accessed: 2019-09-03.

[12] P. Bolzoni, B. A. Kniehl and G. Kramer, Inclusive J/ψ and $\psi(2S)$ production from b-hadron decay in pp and $p\ p$ collisions, Phys. Rev. D 88 (2013) 074035.

[13] B. A. Kniehl, G. Kramer, I. Schienbein and H. Spiesberger, Cross sections of inclusive $\psi(2S)$ and $X(3872)$ production from b-hadron decays in $p\ p$ collisions and comparison with ATLAS, CMS, and LHCb data, Phys. Rev. D 103 (2021) 094002.

[14] M. Butenschoen and B. A. Kniehl, World data of J/ψ production consolidate nonrelativistic QCD factorization at next-to-leading order, Phys. Rev. D 84 (2011) 051501.

[15] S. P. Baranov, A. V. Lipatov and M. A. Malyshev, Associated non-prompt $J/\psi + \mu$ and $J/\psi + J/\psi$ production at LHC as a test for TMD gluon density, Eur. Phys. J. C 78 (2018) 820, arXiv: 1808.06233.

Spin alignment hypothesis corrections

Most general angular dependence for ψ → mu^+mu^- decay:

$$\frac{d^2N}{d\cos\theta^\star d\phi^\star} \propto 1 + \lambda_\theta \cos^2\theta^\star + \lambda_\phi \sin^2\theta^\star \cos 2\phi^\star + \lambda_{\theta\phi} \sin 2\theta^\star \cos\phi^\star$$

- The coefficients λ_θ , λ_ϕ and $\lambda_{\theta\phi}$ are related to the spin-density matrix elements of the dimuon spin wave function for various polarisations.
- It was found that the dependence of acceptance on parameters λ_ϕ and $\lambda_{\theta\phi}$ is very weak, while dependence on λ_θ can be significant.
- In the Tables in the int. note, and in the table in ext note. the correction factors are shown for the extreme polarisation scenarios.

Spin alignment hypothesis corrections

Measurement of the prompt J/ψ and ψ(2S) polarizations in pp collisions at √s = 7 TeV
The CMS collaboration
https://arxiv.org/pdf/1307.6070.pdf

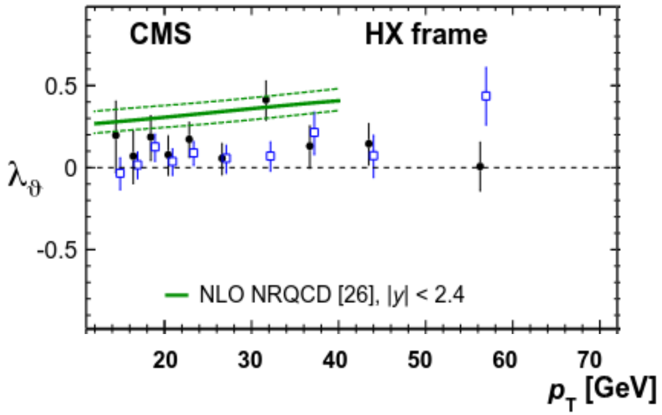

J/ψ Polarization in pp Collisions at √s=7 TeV
B. Abelev et al.*(ALICE Collaboration)
Phys. Rev. Lett. 108, 082001

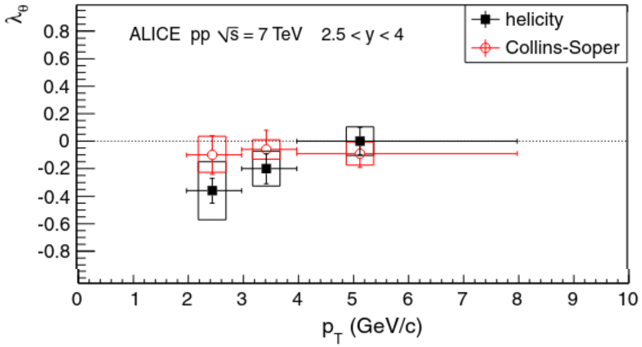

- For illustrating more realistic correction factors, it was decided to produce graphs with correction facors corresponding to the variation of λ_θ between +/-0.2,

  reflecting the level of experimental knowledge on this coefficient.
- Since the spin-alignment corrections are essentially identical for the three rapidity ranges, and also for jpsi and psi2S, it may not be prudent to attach them to each plot, but have them as two separate plots, one for cross sections, and one for non-prompt fractions.

On the polarization of the non-prompt contribution to inclusive J/ψ production in pp collisions

Pietro Faccioli and Carlos Louren
https://arxiv.org/pdf/2206.14686.pdf

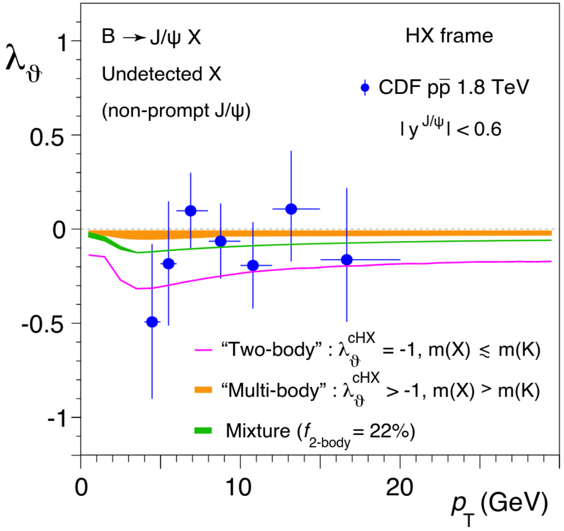

CDF Coll. Phys. Rev. Lett. 85 (2000) 2886

Systematic studies

1) **Acceptance systematics.** Acceptance is a truth-space quantity, and acceptance-related systematics is dominated by the statistics used to generate the corresponding acceptance maps.
   - The maps, that are defined within the range $8 < p$ T $(\mu\mu) < 400$ GeVand $|y(\mu\mu)| < 2.4$, corresponding to the data considered in the analysis.
   - The map is defined in 8 slices in $|y(\mu\mu)|$ and 1000 bins in p T $(\mu\mu)$, using 100k trials for each point, resulting in sufficiently high precision, such that its statistical uncertainty is less than many other sources of systematics.

Systematic studies

2) Trigger efficiency systematics. The systematics on trigger efficiency corrections has a number of components:

1. systematics on correction for trigger efficiency, calculated using MC samples, with respect to reconstructed events.
    - The systematic error for item 1 is calculated in each analysis bin as the binomial error on the ratio of triggered reconstructed events to the number of reconstructed events.
2. systematics on correction for trigger matching, to make sure that the two triggered muons belong to the ψ state.
    - The systematic error for item 2 is calculated in each analysis bin as the binomial error on the ratio of triggered reconstructed events with matched muons to the number of triggered reconstructed events.
3. systematics on correction for trigger scale factor, accounting for differences between the data and MC simulations.
    - The systematic error for item 3 is calculated using the maps provided by the respective performance group, separately for low p T bins with the 2mu4 trigger and high p T bins with the mu50 trigger.

Fractional errors from these three sources in each bin were added in quadrature to form the overall systematic uncertainty for trigger efficiency,

Systematic studies

3) Reconstruction efficiency systematics. In order to correct the observed yields in reconstructed variables to the desired level of true variables, three tasks were performed:

1. the binning in true variables were 'translated' to the binning in reconstructed variables;
2. acceptance defined in true variables were corrected to the level of reconstructed variables;
3. events from the true bin that have not been reconstructed were accounted for.

Using Monte Carlo samples all three tasks were achieved by introducing in each (sub)bin ϵ_{reco}, defined as the ratio of reconstructed events in a reconstructed (sub)bin, with acceptance cuts applied to reconstructed variables $N(RRR)$, over the number of true events in a true (sub)bin with acceptance cuts applied to true variables, $N(TTT)$:

$$\epsilon_{\text{reco}} = \frac{N(RRR)}{N(TTT)} = \frac{N(RRR)}{N(TRR)} \cdot \frac{N(TRR)}{N(TTR)} \cdot \frac{N(TTR)}{N(TTT)}$$

Here:

- the first label states whether the binning is done in true - T or reconstructed - R variables,
- the second – whether the acceptance cuts are applied on true -T or reconstructed - R variables,
- the third – whether the events were reconstruced -R or generated -T.

The final of the three ratios which represents the probability of the event being reconstructed, but in true variables and acceptance, and the first two ratios represent the bin migration, due to variable definition (first) and acceptance cut "correction" (second).

- The systematics were calculated for the three ratios separately, and then combined in quadrature.
- Last part of systematics related to reconstruction is the reconstruction scale factor uncertainty ϵ_{recoSF}. Similarly to the trigger scale factor, the respective systematic error was assessed using the efficiency map scale factors provided by the MCP. This uncertainty was also added in quadrature to form the overall reconstruction systematics.

Reconstruction efficiency systematics

$$\epsilon_{\text{reco}} = \frac{N(RRR)}{N(TTT)} \quad = \frac{N(RRR)}{N(TRR)} \cdot \frac{N(TRR)}{N(TTR)} \cdot \frac{N(TTR)}{N(TTT)}$$

- Being a "proper" efficiency, the third ratio has a binomial uncertainty, which depends on MC statistics in the bin.
- The first and the second ratios are close to identity and their uncertainties are determined by the fidelity of the MC simulated resolutions in p_{T} , which was found to be good.
- The first ratio was found to be scattered in various sub-bins within ±1.5% of the central value, which was applied as a corresponding systematic uncertainty.
- As for the second ratio, It was assessed to be the largest at the low end of p_{T} range, where it reaches 0.7%, and quickly falls at larger p_{T}.

Systematic studies

4) Fit model systematics. There are 14 different variations of the fit model. They are obtained by releasing parameters that were fixed for the nominal variation, one at-a-time. There are 14 fit variations overall:

1. **CB$\boldsymbol{\alpha}$**. The value of the Crystal Ball parameter α was released.

2. **CB$\boldsymbol{n}$**. The value of the Crystal Ball parameter n was released.

3. **CB scale factor**. The value of the Crystal Ball scale factor was released.

4. **Tau resolution $\boldsymbol{\sigma}$**. The value σ of the narrowest Gaussian in lifetime resolution was changed from 0.004 to 0.003.

5. **Tau resolution $\boldsymbol{\mu}$.** The common centre of the three Gaussian in lifetime resolution was released.

6. **$\boldsymbol{\psi(2S)}$ NP fraction**. The fixed value of $\psi(2S)$ non-prompt fraction in the p T bins above 140 GeV is changed from 0.7 to 0.6.

7. **$\boldsymbol{\psi(2S)}$ to $\boldsymbol{J/\psi}$ $\boldsymbol{\sigma}$ scale.** The value of width scale factor between J/ψ and $\psi(2S)$, fixed to their mass ratio, was released.

8. **$\boldsymbol{\psi(2S)}$ to $\boldsymbol{J/\psi}$ $\boldsymbol{\mu}$ scale.** The value of mass scale factor between J/ψ and $\psi(2S)$, fixed to their mass ratio, was released.

9. **$\boldsymbol{\psi(2S)}$ scale factor at high $\boldsymbol{p_T}$** . The fixed value of $\psi(2S)$ to J/ψ cross section ratio in the p T bins above 140 GeV is changed from 0.07 to 0.06.

10. **Correlation $\boldsymbol{\rho}$ = 0**. The value of the correlation factor between the narrowest Gaussians in mass and lifetime was changed from nominal 0.3 to zero.

11. **Tau resolution scale factors**. The values of scale factors between the widths of the three Gaussians in lifetime resolution was changed from 2 and 4 to 3 and 5.

12. **Mass bkg Model 1**. The background model for non-prompt background was changed from the Bernstein polynomials to an exponential.

13. **Mass bkg Model 2**. The background model for prompt background was changed from an exponential to Bernstein polynomials.

14. **$\boldsymbol{\psi(2S)}$ 2nd exp.**. A second exponential was added to the lifetime distribution of $\psi(2S)$.

In each analysis bin, the maximum deviation from nominal yield was divided by √3 and used as an effective symmetric "sigma" for the fit variation systematics.

Systematic studies

5) Luminosity uncertainty.

- High p_T bins: The uncertainty in the combined 2015–2018 integrated luminosity is 1.7%.
- Low p_T bins: The integrated luminosity corresponding to the 2mu4 trigger in 2015 contributes to this measurement with uncertainty of 2.1%

6) Spin alignment correction factors. The polarization of the ψ state may affect acceptance, seven extreme cases that lead to the largest possible variations of acceptance within the phase space of this measurement are identified. These cases are described in the Table. two-dimensional maps are produced for the set of spin-alignment hypotheses.

	Angular coefficients		
	λ_θ	λ_ϕ	$\lambda_{\theta\phi}$
Isotropic *(central value)*	0	0	0
Longitudinal	−1	0	0
Transverse positive	+1	+1	0
Transverse zero	+1	0	0
Transverse negative	+1	−1	0
Off-(λ_θ–λ_ϕ)-plane positive	0	0	+0.5
Off-(λ_θ–λ_ϕ)-plane negative	0	0	−0.5

Values of angular coefficients describing the considered spin-alignment scenarios.

This analysis adopts the isotropic distribution in both cos $\theta^\star$ and $\phi^\star$ as nominal, and the variation of the results for a number of extreme spin-alignment scenarios is studied and presented as sets of correction factors (Appendix K).

$\theta^\star$ - angle between the direction of the positive-muon momentum in the ψ rest frame and the momentum of the ψ in the laboratory frame.

$\phi^\star$ - angle between the dimuon production and decay planes in the laboratory frame.

The ψ production plane is defined by the momentum of the ψ in the laboratory frame and the positive z-axis direction.